Surface-Center Temperature Differences Within Milk Droplets During Convective Drying and Drying-Based Biot Number Analysis

Kamlesh C. Patel
Biotechnology and Food Engineering Group, Dept. of Chemical Engineering, Monash University, Clayton Campus, Victoria 3800, Australia

Xiao Dong Chen
Biotechnology and Food Engineering Group, Dept. of Chemical Engineering, Monash University, Clayton Campus, Victoria 3800, Australia

Dept. of Chemical and Materials Engineering, Private Bag 92019, University of Auckland, Auckland 1010, New Zealand

DOI 10.1002/aic.11608
Published online November 4, 2008 in Wiley InterScience (www.interscience.wiley.com).

An assumption of uniform temperature is frequently used when evaluating average temperature-time and average moisture content-time profiles for the convective drying of small droplets or thin-layer materials. In most studies, the assumption of uniform temperature was justified by estimating the heat-transfer Biot number at the beginning and end of the drying process. However, the conventional Biot number analysis performed in the literature does not reflect the evaporative effect. In this article, we have examined the temperature uniformity and the heat-transfer Biot number during the drying of skim milk droplets under laboratory drying conditions following the entire drying process. Surface-centre temperature differences and conventional and drying-based Biot numbers are calculated during the drying of skim milk droplets. A simple procedure is outlined to estimate the extent of temperature nonuniformity within the droplet. Results demonstrated that temperature nonuniformity within the skim milk droplets under drying conditions examined is very small, thus the uniform temperature assumption is more likely to be a reliable approach to model heat and mass transfer processes in industrial spray dryers. The analyses provided in this study help in understanding a few assumptions used in literature, and offer a framework that may be used in the future. © 2008 American Institute of Chemical Engineers *AIChE J,* 54: 3273–3290, 2008

Keywords: biot number, spray drying, droplet drying, modeling, temperature distribution

Introduction

Spray drying is a widely used industrial operation that involves evaporation of moisture from droplets until the desired particle moisture content is achieved. A mathematical analysis to characterize the drying of individual droplets is important because it provides a more intelligent and robust control over the product quality and the plant operation. A simple approach to achieve the expected product quality during spray drying can be formulated by recognizing what the droplet/particle experiences during its transit in the drying chamber.[1] The physical and biochemical properties of the

Correspondence concerning this article should be addressed to Xiao Dong Chen at dong.chen@eng.monash.edu.au.

final dried product are directly influenced by the droplet's temperature and moisture content history within the dryer. Hence, predicting the droplet's temperature-time and moisture concentration-time profiles following the entire drying operation is crucial for manufacturing the best-quality product and optimizing the operation.

During spray drying, the evaporation from droplets is facilitated by mixing hot drying gas with a spray of small droplets. Droplets receive the heat from drying gas, and subsequently moisture is transferred from the droplets to the bulk gas in the form of vapor. The driving force for these heat and mass transfer processes may be the liquid moisture concentration difference, the vapor pressure difference, or the temperature difference within and outside the droplet. The transport of heat and moisture may lead to nonuniformity of temperature, pressure, and moisture concentration inside the droplet/particle depending on the size and physical and biochemical properties. Nonuniformity within the droplet may influence several thermo-physical properties of the product, for example, glass transition temperature as well as product characteristics such as stickiness and agglomeration. This influence primarily depends on the extent of nonuniformity. If the magnitude of nonuniformity is small, the uniform conditions within the droplet may be assumed during modeling without introducing significant errors in predictions.

There have been several studies previously published on modeling heat and mass transfer processes during the air drying of single droplets, particles, and thin layer materials.[2–15] In industrial spray drying operations, the initial droplet diameter usually varies from 10–500 μm. The maximum diameter is often used to perform mathematical modeling and to develop the theory.[4] Mathematical models were mainly validated using laboratory data collected from 1–3 mm size droplets or thin slabs.[4–7,11–15] Several assumptions were introduced to simplify mathematical analysis. Assuming negligible temperature distribution inside small droplet or thin slab has been a common approach in most studies.[2,4,8–11,13] Application of this assumption offers advantages such as reducing computation time and making the drying models more compatible with commercial CFD packages such as Fluent and CFX to track thousands of particles in the real process that involves a wide particle size distribution. So far there has been no rigorous assessment of the uniform temperature assumption following the entire drying operation.

The main objective of this article is to estimate surface-centre temperature differences as well as heat-transfer Biot numbers following the complete droplet drying process to check the extent of temperature nonuniformity within the droplet/particle. Both conventional and drying-based Biot numbers are calculated and compared to check their appropriateness under drying circumstances. To calculate surface-center temperature differences under drying conditions, an approximation method is worked out in this article. Experimental data on the drying of skim milk droplets reported by Lin[15] were used in this work. Skim milk is a complex biological material and has been widely used to study the drying behavior, hence chosen as a typical material for this work. The shrinkage effect was taken into account during modeling. The proposed method was also used to deliver surface-center temperature predictions for micron-sized droplets under industrial spray drying conditions. The analyses presented in this article offer a first estimate to decide whether the uniform temperature assumption is reasonable during the fast drying of small droplets or porous particles.

Basic Modeling Approaches Considered in Literature

In this section, the existing models on the air drying of droplets containing dissolved solids and porous particles are briefly reviewed. Key equations for each approach are presented in this section to highlight the fundamental concept and to be used in the later analysis.

The first modeling approach assumed uniform temperature within the droplets.[2,8,10,11,13,15–17] The moisture concentration distribution effect was taken into account by using lumped-parameter models, such as the characteristic drying rate curve (CDRC) model and the reaction engineering approach (REA).[11,13,15,17] The following heat transfer model was used to estimate the temperature-time profile:

$$\frac{d\overline{T}_{\mathrm{p}}}{dt} = \frac{hA_{\mathrm{p}}(T_{\mathrm{b}} - \overline{T}_{\mathrm{p}}) + \Delta H_{\mathrm{L}} \cdot m_{\mathrm{s}} \frac{d\overline{X}}{dt}}{m_{\mathrm{s}} C_{\mathrm{p,s}} + m_{\mathrm{w}} C_{\mathrm{p,w}}} \tag{1}$$

where h (W m^{-2} K^{-1}) is the convective heat-transfer coefficient, A_{p} (m^2) is the droplet surface area, T_{b} (K) is the bulk gas temperature, $\overline{T}_{\mathrm{p}}$ (K) is the average droplet temperature, ΔH_{L} (J kg^{-1}) is the latent heat of vaporization, m_{w} and m_{s} (kg) are mass of water and solids, and $C_{\mathrm{p,w}}$ and $C_{\mathrm{p,s}}$ (J kg^{-1} K^{-1}) are specific heat capacity of water and solids, respectively. Both CDRC and REA models coupled with Eq. 1 have been found attractive for modeling large-scale operations mainly due to its simplicity (as it requires only time integration) and its fairly reasonable accuracy in predicting drying parameters and product quality.

The second modeling approach assumed uniform temperature within the droplet, but solved for detailed moisture concentration distribution inside the droplet.[3,4,7,9,18–20] The internal moisture transport was considered as a rate-limiting process by assuming that the internal heat transport takes place very quickly compared to the internal mass transport. The spatial moisture distribution within the droplet or the porous particle was mainly estimated using the effective diffusivity-based drying kinetics model.[3,4,7,9,18–20] If the shrinkage behavior and the deformation of the material are considered during modeling, this diffusion model and its numerical solution become extremely complicated. The effective diffusivity (m^2 s^{-1}), which is a material-dependent property and is a function of temperature and moisture content,[6] was used to account for the overall transport of moisture during the entire drying process. Equation 1 was normally used to estimate the droplet's temperature profile. In spite of the complexity of the model and the difficulty in obtaining the effective diffusivity, the modeling approach that assumed uniform temperature within the droplet and solved for internal moisture distribution has performed reasonably well in dryer-wide simulations.

The third modeling approach is based on a receding interface model (or moving boundary approach), which solved to evaluate the spatial distribution of temperature and/or moisture concentration within the droplet.[5,12,21–28] Most of the

work published to date for estimating internal temperature gradients is based on the receding interface approach. When estimating internal moisture distribution using this approach, most studies considered the drying of the hygroscopic material to be mass-transfer limiting where the uniform temperature within the droplets may still be used.[24,26,27] On the other side, Farid[12] proposed the model (i.e. heat-transfer limiting theory) to evaluate temperature distribution within the droplets claiming the drying process to be heat-transfer limiting.

A range of assumptions were used when formulating the drying kinetics model using the receding interface approach. For instance, Cheong et al.[5] and Dolinsky[25] assumed a linear temperature distribution in the crust of the material, and uniform temperature throughout the wet core. Kuts et al.[26] assumed the crust-wet core interface temperature to be constant and equal to the corresponding wet-bulb temperature of hot air. The initial warm-up period during the droplet drying process was neglected by Dolinsky[25] and Kuts et al.[26] Farid[12] neglected the mass transfer resistance during modeling the internal heat transport. The internal temperature distribution was mainly calculated using the following heat conduction equation[12]:

$$\frac{\partial T}{\partial t} = \frac{\alpha}{r^2}\left[\frac{\partial}{\partial r}\left(r^2 \frac{\partial T}{\partial r}\right)\right] \tag{2}$$

Equation 2 was solved using the following boundary conditions:

$$\frac{dT}{dr} = 0 \quad \text{at } r = 0 \tag{3}$$

$$-k_p \frac{dT}{dr} = h(T_s - T_s) \quad \text{at } r = R \tag{4}$$

where α ($m^2\ s^{-1}$) is the thermal diffusivity, R (m) is droplet radius, r (m) is the radial distance within the droplet, k_p (W $m^{-1}\ K^{-1}$) is the droplet's thermal conductivity, and T_s (K) is the droplet's surface temperature. The overall change in the droplet weight during drying was calculated assuming the mass of solids and bound water remained constant during the entire drying period[12]:

$$\text{Mass} = \frac{4}{3}\pi {R_s}^3 \rho_p (1 - w_0) + \frac{4}{3}\pi {R_i}^3 \rho_p (w_0 - w_b) + \frac{4}{3}\pi {R_s}^3 \rho_p w_b \tag{5}$$

where R_s is the droplet radius after shrinkage and R_i the radius at the core-crust interface. The first and third terms on the right hand side of the Eq. 5 were mass of solids and bound water, respectively. The second term was the mass of free water that is available for evaporation. Hence, there was no drying kinetics involved during modeling the droplet's weight-loss profile. The heat-transfer limiting theory proposed by Farid[12] has shown large errors when predicting average temperature and average moisture content profiles for the air drying of 20 wt % skim milk droplets of 1.9 mm initial diameter.

Because the heat-transfer limiting theory estimated a largest extreme of surface-centre temperature differences (over 10°C), the theory is analyzed here in depth with respect to spray drying of individual droplets. In the original heat-transfer limiting theory, the entire drying process was partitioned into four distinct stages[12]:

Initial warm-up period

The first stage was set for the sensible heating of the droplet where the droplet's surface temperature reached the wet-bulb temperature of drying gas. The heat transfer model, presented by Eq. 2, was solved using the boundary conditions (Eqs. 3 and 4) to estimate the droplet temperature profile. The evaporation rate was assumed to be zero during this initial warm-up period.

Constant and uniform wet-bulb temperature period

Once the droplet reached the wet-bulb temperature, the droplet experienced evaporation until there was "zero" free moisture on the droplet surface. The droplet temperature remained at the wet-bulb temperature throughout this period. The temperature within the droplet was assumed to be uniform. Hence, no models were needed to predict the droplet temperature for this period. The droplet was assumed to experience shrinkage only during this period.

Crust formation period

After the constant and uniform wet-bulb temperature period, the crust formation was commenced on the droplet surface due to zero free water on the droplet surface. Shrinkage was assumed to be stopped as soon as the crust formed on the droplet surface. The partially dried particle was divided into two main regions: the outer dry crust and the inner wet core, separated by a sharp moving boundary (receding interface). Evaporation was assumed to occur only from this moving boundary. The dry crust was assumed to have constant "bound" moisture that cannot be removed anymore, whereas the moving boundary and the wet core were assumed to be fully saturated with the water. Again the same heat conduction model (Eq. 2) was solved using the same boundary conditions (Eqs. 3 and 4) for the dry crust and the wet core separately. This drying stage continued until the dry crust reached the centre of the particle. Mezhericher et al.[28] assumed the crust thermal conductivity to be temperature independent when estimating the crust temperature in this period.

Final sensible heating period

The final stage was set for another sensible heating of the completely dry particle. During this final stage, the temperature distribution inside the dried particle was estimated using Eqs. 2–4 by taking into account only the crust thermo-physical properties. The dried particle was assumed to have constant bound moisture content at the end of the drying process irrespective of drying gas conditions.

Several disagreements exist in the predictions illustrated by Farid.[12] For instance, predicted droplet temperature profiles by Farid[12] for the drying of 20 wt % skim milk droplets demonstrated that the estimated droplet temperature was in fact not constant during the assumed constant wet-bulb temperature period. In a way, the constant temperature assumption used during the theory development was not executed

during the simulation. Several limitations of the receding interface approach are briefly discussed here.

It is common in industries to spray the liquid milk with 50–55 wt % initial solids contents and 50–60°C initial feed temperatures. For droplets of such high initial temperatures (higher than the air wet-bulb temperature), the droplet surface temperature has to be reduced towards the evaporation temperature. The droplet should experience some evaporation during this evaporation temperature adjustment. This is supported by the experimental work of Cheong et al.[5] and Lin[15,29] on the hot air drying of single droplets. Therefore, the assumption of no evaporation during the first drying stage by the heat-transfer limiting theory may not be generalized.

The second drying period may not exist for materials having high initial solids contents (i.e. negligible constant drying rate period) because the droplet's surface temperature after the initial wet-bulb temperature adjustment would rise continuously and quickly due to a reduction in free moisture at the droplet surface. For materials which do not exhibit the constant drying rate period, the heat-transfer limiting theory would yield no change in the droplet diameter during drying because the shrinkage was set to happen only during the constant drying rate period. In fact, the shrinkage has been shown to occur until later stages during the drying of single, suspended skim milk and whole milk droplets under constant air temperature and humidity conditions.[29]

A very abrupt fall in moisture concentrations at the receding interface is always expected for the receding interface approach because the wet core and the receding interface were assumed to have saturated water concentrations, whereas the dry crust had constant, yet very small bound water content. In fact porous materials such as skim milk and whole milk solids have high affinity to absorb moisture, and hence some moisture distribution is expected between the dry outer surface and the wet saturated core.[30] Schrader and Litchfield[31] studied the moisture concentration profile in a model food gel during drying using a magnetic resonance imaging technique, and confirmed that there is no sharp interface between the wet and dry regions on which evaporation occurs. The work of Cheong et al.[4] is an evident for the above phenomenon. Cheong et al.[4] assumed that evaporation occurs only on the sharp interface during modeling for the drying of aqueous sodium sulphate decahydrate droplets. The prediction by Cheong et al.[4] illustrated that the formulated model overestimated the droplet weight profile after the crust formed on the droplet surface. This means the predicted droplet weight (after the crust formation) was higher than the measured one. This observation favors that the evaporation should occur in certain regions between the droplet outer surface and the wet core rather than only on the sharp interface. In essence, the assumption of moisture evaporation only from the receding interface may not be suitable for the drying of hygroscopic porous materials.

As mentioned previously, the outer dry crust was assumed to have prefixed bound water. This generalization does not reflect the principle of the "equilibrium" moisture content.[6,11,28] Whitaker[32] studied the gas-phase convective transport during the drying of the porous material and showed that the moisture gradient should be present in the dry crust region. This phenomenon is supported by Chen and Pei,[6] who illustrated that the moisture migrates within the crust due to the flow along very fine capillaries or through the cellular membranes during the drying of hygroscopic materials. This moisture movement generates transitional moisture distribution in the crust region. Bramhall[33] demonstrated that the bound water cannot be assumed constant because some bound water molecules receive enough energy to break the sorptive bonds. These free molecules can migrate in the dry crust until captured by the other sites or may be evaporated. These experimental studies suggest that the assumption of the crust having a constant bound moisture profile may not be appropriate. In general, under a moderate temperature range, it is expected that the mass-transfer resistance should play a role during drying. The "pure" heat-transfer limiting drying process is likely to be an extreme consideration when drying hygroscopic porous materials.

An Approximation Procedure to Evaluate Surface-Center Temperature Differences

In this section, an approximation procedure is outlined to estimate surface-centre temperature differences within small hygroscopic droplets under drying conditions. This method may also be used for the drying of materials in a thin slab form. The same authors made an attempt earlier to establish such procedures;[34] however, it fell short in terms of the solution being incorrect. In this article, a more profound approximation procedure is presented which will be of significant importance when modeling heat and mass transfers in multiphase flows. The drying of acqueous droplets is assumed here to start with the evaporation of water from the droplet surface. When the droplet surface is fully covered with water, the drying rate would be similar to the rate for pure water evaporation. For the droplet that contains dissolved or suspended solids, the vapor pressure at the droplet surface would become smaller than that of the pure water droplet when there is not enough free moisture on the surface. As a result, the mass transfer rate will be reduced as the drying of the moist droplet proceeds further. Once the surface vapor concentration falls below the saturated vapor concentration corresponding to the surface temperature, the drying also commences within the droplet. This leads to the formation of a porous solid phase near the surface region. The solid dry crust provides a resistance to the heat and mass transport to and from the droplet. As a consequence, the droplet's surface temperature will increase above the evaporation temperature corresponding to drying gas conditions.

The temperature gradient within the droplet can be evaluated by balancing the heat for the droplet-air system. The following unsteady-state heat conduction equation and boundary conditions may be used for the spherical coordinate system (r, t):

$$\frac{1}{r^2}\frac{\partial}{\partial r}\left(k_p r^2 \frac{\partial T}{\partial r}\right) = \rho C_p \frac{\partial T}{\partial t} \tag{6}$$

Boundary Condition 1

$$\text{At } r = 0, \quad \frac{\partial T}{\partial r} = 0 \tag{7}$$

Boundary Condition 2

$$\text{At } r = R, \quad k_p \frac{dT}{dr} = \overline{h}(T_b - T_s) - \Delta H_L \overline{N}_v \tag{8}$$

where $\overline{N}_v$ (kg m^{-2} s^{-1}) is the evaporation flux, $\overline{\rho}$ (kg m^{-3}) is average droplet density and $\overline{C}_p$ (J kg^{-1} K^{-1}) is average heat capacity of the droplet. The latent heat of vaporization (ΔH_L, J kg^{-1}) was estimated at atmospheric pressure conditions using the following Watson correlation[35]:

$$\Delta H_L = \Delta H_{L,ref}\left(\frac{1-(T/647.1)}{1-(T_{ref}/647.1)}\right)^{0.38} \tag{9}$$

where T is the absolute local temperature (K). The latent heat of vaporization was estimated using the reference condition: T_{ref} = 273.15 K, $\Delta H_{L,ref} = 2500 \times 10^3$ J kg^{-1}.[36]

The temperature change with respect to time ($\partial T_p/\partial t$) may be approximated by plotting the measured droplet temperature T_p (traditionally taken as average temperature, $\overline{T}_p$) against time t. For the individual time step, the term on the right hand side of Eq. 6 may be considered constant because individual average properties of the droplet will remain constant for that particular time step. Under these circumstances, Eq. 6 can be rewritten in its integral form when taking $\rho \cdot C_p$ as average values, that is $\overline{\rho} \cdot \overline{C}_p$:

$$\int \frac{\partial}{\partial r}\left(k_p r^2 \frac{\partial T}{\partial r}\right)dr \approx \overline{\rho}\overline{C}_p \frac{\partial \overline{T}_p}{\partial t}\int r^2 dr \tag{10}$$

Equation 10 can be rewritten as:

$$r^2 \frac{\partial T}{\partial r} = \frac{\overline{\rho}\overline{C}_p}{k_p}\frac{\partial \overline{T}_p}{\partial t}\frac{r^3}{3} + \frac{C_1}{k_p} \tag{11}$$

where C_1 is an integration constant. If we use $k_p \approx \overline{k}_p$ for simplicity, we can introduce the average thermal diffusivity ($\overline{\alpha} = \overline{k}_p/\rho\overline{C}_p$) to Eq. 11. Because the thermal conductivity of the small single droplet is difficult to measure from independent experiments, the "mean" thermal conductivity ($\overline{k}_p$) estimated using equations presented by Choi and Okos[37] was used in this study. The $\overline{k}_p$ estimation procedure is presented in Appendix A. The integration constant C_1 can be obtained using the first boundary condition presented by Eq. 7. On application of this boundary condition, we find C_1 to be zero, thus giving:

$$\frac{\partial T}{\partial r} = \frac{1}{\overline{\alpha}}\frac{\partial \overline{T}_p}{\partial t}\frac{r}{3} \tag{12}$$

Equation 12 can be written in the following integral form:

$$\int \frac{\partial T}{\partial r}dr = \frac{1}{\alpha}\frac{\partial \overline{T}_p}{\partial t}\int \frac{r}{3}dr \tag{13}$$

With the incorporation of the second integration constant C_2, Eq. 13 can be rewritten as:

$$T(r) = \frac{1}{\overline{\alpha}}\frac{\partial \overline{T}_p}{\partial t}\frac{r^2}{6} + C_2 \tag{14}$$

$$\text{At } r = R \quad T_s = \frac{1}{\overline{\alpha}}\frac{\partial \overline{T}_p}{\partial t}\frac{R^2}{6} + C_2 \tag{15}$$

To evaluate the second integration constant C_2, the second boundary condition was used. By combining Eqs. 8, 12, and 15, we obtain

$$\frac{\overline{k}_p}{3\overline{\alpha}}\frac{\partial \overline{T}_p}{\partial t}R = \overline{h}\left(T_b - \frac{1}{\overline{\alpha}}\frac{\partial \overline{T}_p}{\partial t}\frac{R^2}{6} - C_2\right) - \Delta H_L \overline{N}_v \tag{16}$$

From Eq. 16, the integration constant C_2 can be expressed as:

$$C_2 = T_b - \frac{1}{\overline{\alpha}}\frac{\partial \overline{T}_p}{\partial t}\frac{R^2}{6} - \frac{1}{\overline{h}}\left(\frac{\overline{k}_p}{3\overline{\alpha}}\frac{\partial \overline{T}_p}{\partial t}R + \Delta H_L \overline{N}_v\right) \tag{17}$$

By inserting C_2 in Eq. 14, we obtain

$$T(r) = \frac{1}{\overline{\alpha}}\frac{\partial \overline{T}_p}{\partial t}\frac{r^2}{6} + \left[T_b - \frac{R^2}{6\overline{\alpha}}\frac{\partial \overline{T}_p}{\partial t} - \frac{1}{\overline{h}}\left(\frac{R\overline{k}_p}{3\overline{\alpha}}\frac{\partial \overline{T}_p}{\partial t} + \Delta H_L \overline{N}_v\right)\right] \tag{18}$$

This model, presented by Eq. 18, provide a parabolic temperature profile within the droplet/particle. The model clearly shows the dependency of the droplet temperature on the rate of change of temperature. At $r = 0$, Eq. 18 will give:

$$T_c = \left[T_b - \frac{R^2}{6\overline{\alpha}}\frac{\partial \overline{T}_p}{\partial t} - \frac{1}{\overline{h}}\left(\frac{R\overline{k}_p}{3\overline{\alpha}}\frac{\partial \overline{T}_p}{\partial t} + \Delta H_L \overline{N}_v\right)\right] \tag{19}$$

It can be observed that the second integration constant C_2 is essentially the droplet/particle's centre temperature (T_c). Then the expression to estimate surface-centre temperature differences (ΔT) during the drying of single droplets/particles can be obtained using Eq. 15:

$$\Delta T = T_s - T_c = \frac{R^2}{6\overline{\alpha}}\frac{\partial \overline{T}_p}{\partial t} \tag{20}$$

From the above model, we can approximate that the surface-centre temperature difference is directly proportional to the rate of change of the droplet's average temperature ($\partial \overline{T}_p/\partial t$) as well as surface area (R^2). The influence of the drying rate on ΔT is indirectly reflected by the ($\partial \overline{T}_p/\partial t$) term. Equation 20 illustrates that estimating the surface-centre temperature difference requires an accurately measured temperature-time profile ($\partial \overline{T}_p/\partial t$) over the entire drying process.

Biot Numbers Analysis

A justification of the assumption of uniform temperature was traditionally provided by estimating the heat-transfer Biot number (Bi) at the beginning and end of the drying process. To neglect the temperature distribution within the droplet, the heat-transfer Biot number is conventionally required to be less than a critical value of 0.1.[12,38–40] It should be noted that this critical value of 0.1 is not an absolute measure and it is used as a relative "yard-stick". This critical value can be made even smaller (say 0.01) depending on the tolerance to the idea of acceptable "temperature uniformity."

For nonevaporative conditions (i.e. heating only scenario), the heat-transfer Biot number is generally expressed as a ratio of the internal conduction resistance to the external convection resistance:

$$Bi = \frac{R_c/\overline{k}_p}{1/\overline{h}} = \frac{\overline{h}R_c}{\overline{k}_p}, \quad \text{where } R_c \approx R \tag{21}$$

Here, $\overline{h}$ (W m^{-2} K^{-1}) is the average heat-transfer coefficient, $\overline{k}_p$ (W m^{-1} K^{-1}) is the droplet's mean thermal conductivity,

Table 1. Initial Drying Conditions for the Air-Drying of 30 wt % Skim Milk Droplets of 1.45 mm Initial Diameter

Case No.	Drop Diameter (mm)	Drop Temperature (°C)	Air Dry-Bulb Temperature (°C)	Air Wet-Bulb Temperature (°C)	Air Velocity (m s^{-1})	Air Humidity (g kg^{-1}, dry basis)
A	1.45	28.6	67.5	23.4	0.45	0.1
B	1.45	25.4	67.5	23.4	1.00	0.1
C	1.45	31.8	87.1	28.5	0.45	0.1
D	1.45	29.8	87.1	28.5	1.00	0.1
E	1.45	30.8	106.6	32.0	0.45	0.1

and R_c (m) is the droplet's characteristic radius. The characteristic radius R_c is normally related to the length scale corresponding to the maximum spatial temperature difference. For small droplets, R_c is generally taken as 1/3 of the droplet radius (R). However, for a large sphere, R_c may be taken as the same as the droplet radius.[40] In this work, the droplet radius R is used as R_c to estimate the Biot numbers, so that the maximum extent of the Biot numbers may be evaluated.

At the beginning of the droplet drying process, Bi is likely to be small due to high water content and thus relatively large $\overline{k}_p$. During the later drying stage, a major portion of the water is transferred from the droplet to the bulk drying gas leading to a reduction in $\overline{k}_p$. Another reason for the reduced $\overline{k}_p$ is the porous structure development within the particle possibly filled with air and vapor, which have relatively low thermal conductivity. Because Bi is inversely proportional to $\overline{k}_p$, Bi is expected to become larger as drying proceeds. It is therefore possible that the calculated Bi could exceed the critical value of 0.1, and consequently the temperature gradient inside the particle is said not to be negligible. As an example, the initial thermal conductivity of the 20 wt % skim milk droplet of 1.9 mm initial diameter was considered as 0.55 W m^{-1} K^{-1} during calculating Bi by Farid.[12] The initial value of Bi was reported to be around 0.15. At the end of drying, Bi was shown to be increased by one order of magnitude (higher than 1.0) by adjusting the final $\overline{k}_p$ to be 0.07 W m^{-1} K^{-1}. In this way, the uniform temperature assumption was said to be invalid because the predicted Bi largely exceeded the critical value at the end of drying.

The classical Biot number does not consider the evaporative effect, thus it was suspected not to be a good reflection of the droplet drying process. A drying-based Biot number has recently been developed by Chen and Peng[41] to account for the evaporative effect during the droplet drying process:

$$Bi^{\#} = Bi - \frac{\Delta H_L \overline{N}_v}{(T_b - T_s)} \frac{R}{\overline{k}_p} \tag{22}$$

where $Bi^{\#}$ is the drying-based Biot number, Bi is the conventional Biot number, and T_b and T_s are drying gas and droplet surface temperatures (K), respectively. The second term on the right hand side of Eq. 22 should be taken into account when the evaporation plays a significant role in removal of moisture. Based on this new definition, $Bi^{\#}$ is expected to be smaller than the one estimated using the conventional theory. The drying-based Biot number also suggests that the temperature gradient within the droplet may not be as large as perceived by the conventional approach.

Results and Discussion

The analytical solution of the unsteady-state heat conduction equation is presented in the earlier section. Simulations were carried out using Microsoft Excel (2003 professional edition) spreadsheets. Surface-centre temperature differences and both conventional and drying-based Biot numbers are estimated in this section for the drying of 30 wt % skim milk droplets of 1.45 mm initial diameter using five sets of experimental conditions (Cases A to E) reported in Table 1. The droplet's temperature-time and diameter-time profiles and other required parameters such as heat-transfer coefficients were obtained from accurate experimental measurements reported by Chen and Lin[13] and Lin[15] on the convective drying of skim milk droplets. Hot air of constant temperature, humidity, and velocity was used to evaporate moisture from the droplets. A detailed description of the equipment, the measurement technique, and the data analysis can be obtained from the various published literature.[13,15,29,42] In the experimental work of Chen and Lin[13] and Lin,[15] the accuracy of weight and temperature measurements was reported to be ± 0.05 mg and ± 0.1°C, respectively. The measured droplet temperature from the droplet drying experiment was assumed here as the average droplet/particle temperature. Skim milk solids were considered to be made of 49.8% lactose, 36.5% total proteins, 0.6% fat, 9.3% minerals, and 3.8% moisture (all weight percentages).[13,43]

Predicting the average thermal conductivity

The mean thermal conductivity of skim milk droplets were estimated using two models, one that does not consider the porosity in the particle structure and another that takes into account the porosity. Porosity of the dried particle is a material-dependent property, and a complex function of the material's temperature and moisture content. Because it is extremely difficult to evaluate the transient change in the porosity for a single small-size droplet during drying, the model presented by Eq. A3 and A4 has integrated the final porosity value from the beginning of the drying process. This approach provided two bounds of the mean thermal conductivity ($\overline{k}_p$) shown in Figure 1 for Case-A to Case-E drying circumstances.

The predicted profiles without porosity (see the higher bound in Figure 1) illustrates that $\overline{k}_p$ of the skim milk droplets at the beginning of drying is estimated to be 0.50 W m^{-1} K^{-1}, whereas it was approximately 0.41 W m^{-1} K^{-1} at the end of drying. Because the porosity of the droplet at the beginning of drying is negligible, the higher bound of the thermal conductivity would provide accurate values for the earlier drying stage. The mean thermal conductivity profiles which take into account the porosity effect during drying are shown by a lower bound in Figure 1. For the fully dried skim milk powder, the porosity of the single dried particle was reported to be ~0.163 at 50°C conditions.[41] It can be observed from the Figure 1 (see the lower bound) that $\overline{k}_p$ of skim milk droplets

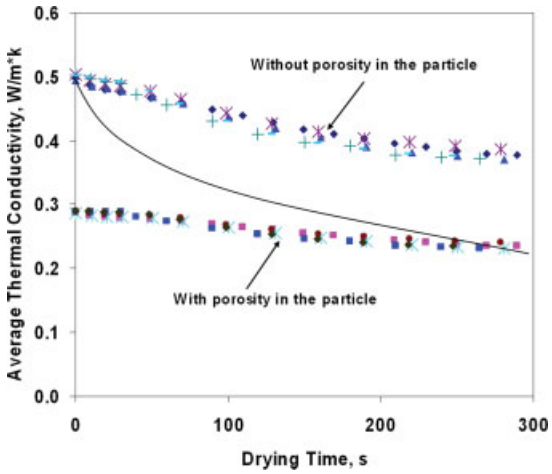

Figure 1. Average thermal conductivity profiles during drying for the 30 wt % skim milk droplets of 1.45 mm initial diameter using Case-A to Case-E drying conditions.

[Color figure can be viewed in the online issue, which is available at www.interscience.wiley.com.]

was ~0.3 W m^{-1} K^{-1} at the beginning of drying, whereas it was around 0.25 W m^{-1} K^{-1} at the end of the process. It should be noted that the lower bound of $\bar{k}_p$ would provide accurate values during later stages of drying where the porosity effect is more significant.

The true thermal conductivity profile of skim milk droplets during drying may be traced between higher and lower bounds as highlighted by a full line in Figure 1. Thus, the initial $\bar{k}_p$ of the skim milk droplet would be 0.50 W m^{-1} K^{-1}, and $\bar{k}_p$ at the end of drying can be considered as 0.25 W m^{-1} K^{-1}. It would be interesting to evaluate ΔT and both conventional and drying-based Biot numbers using higher and lower thermal conductivity bounds. The higher bound of $\bar{k}_p$ is likely to result in a lower extreme of ΔT and Biot numbers, whereas the lower bound of $\bar{k}_p$ would yield a higher extreme.

Predicting the surface-center temperature difference

The surface-center temperature difference (ΔT) profile is predicted by Eq. 20 using two bounds of $\bar{k}_p$. The real ΔT profile is likely to occur between these high extreme ΔT profile (low $\bar{k}_p$ bound) and low extreme ΔT profile (high $\bar{k}_p$ bound). Predicted surface-centre temperature difference profiles and measured average moisture content and temperature profiles of skim milk droplets for Case-A to Case-E drying conditions are presented in Figure 2. The maximum of surface-centre temperature difference (ΔT_{max}) using both thermal conductivity bounds are presented in Table 2 for the same droplet and drying conditions.

In general, the surface-centre temperature difference (ΔT) was observed to be less than 0.7°C for the air drying of 30 wt % skim milk droplets of 1.45 mm initial diameter. On the other hand, the heat-transfer limiting model predicted the surface-core temperature difference over 10°C for the air drying of 20 wt % skim milk droplets of 1.9 mm initial diameter using the hot air of 70°C temperature and 1.0 m s^{-1} velocity.[12] Predictions in this study using the similar droplet and air conditions (refer to Case-A and Case-B conditions) demonstrated that maximum temperature gradients (ΔT_{max}) within skim milk droplets were less than 0.7°C using both high and low thermal conductivity bounds (see Table 2).

It can be observed from the Figure 2a (Case-A drying conditions) that ΔT was negative during the earlier drying stage. For the Case-A, the initial droplet temperature was 28.6°C that was higher than the surrounding air wet-bulb temperature (23.4°C). Therefore, the droplet surface temperature reduced to the evaporation temperature that is close to the air wet-bulb temperature. The droplet could have negative ΔT during this period due to the flow of the heat from the centre to the surface. Interestingly, the droplet should have experienced some evaporation when the surface temperature was reduced close to the wet-bulb temperature. Hence, an assumption of no evaporation during the first drying period may not be generalized as done by the receding interface approach. For the Case-B to Case-D drying processes, the initial droplet temperature was smaller than the corresponding air wet-bulb temperature by less than 2°C, and the negative ΔT therefore did not exist.

It can be noticed from the Figure 2 that ΔT is relatively high during the earlier drying stage where the porosity effect in the droplet may be insignificant. This indicates that the maximum temperature difference (ΔT_{max}) predicted by the model that neglected the air porosity (high $\bar{k}_p$ bound predictions) are more accurate. Predictions of ΔT also demonstrate that ΔT_{max} was bigger for higher air temperature conditions. This trend was observed for both air velocity conditions (see Table 2). At the same air temperature condition, ΔT_{max} was bigger for higher initial air velocity conditions. These findings suggest that the initial temperature and velocity of drying gas can influence the average drying rate, the rate of change of droplet temperature and also the droplet's surface properties such as temperature and moisture content.

It is important to know where and when maximum temperature differences (ΔT_{max}) occur during industrial spray drying operations because the droplet's surface properties may have significant influence on wall deposition and overall product quality. During the droplet drying process considered in this study, the constant wet-bulb temperature period was very small (see drop temperature profiles in Figure 2). The droplet temperature significantly increased straight after the droplet temperature reached the wet-bulb temperature, indicating the onset of the crust formation on the droplet surface. In this study, maximum temperature gradients (ΔT_{max}) within skim milk droplets/particles were observed immediately after the evaporation temperature adjustment period or when the crust formation commenced on the droplet surface. In industrial spray dryers, if the maximum temperature gradient within the droplets occurs near the atomization zone or far away from the dryer wall, the temperature nonuniformity may not influence the deposition of aqueous materials on the dryer wall.

It is clear from all the simulation results that surface-centre temperature differences during the drying of skim milk droplets under laboratory drying conditions (i.e. constant air temperature and humidity conditions) were less than 0.7°C. In contrast, the heat-transfer limiting model estimated large ΔT by setting the particle crust thermal conductivity to

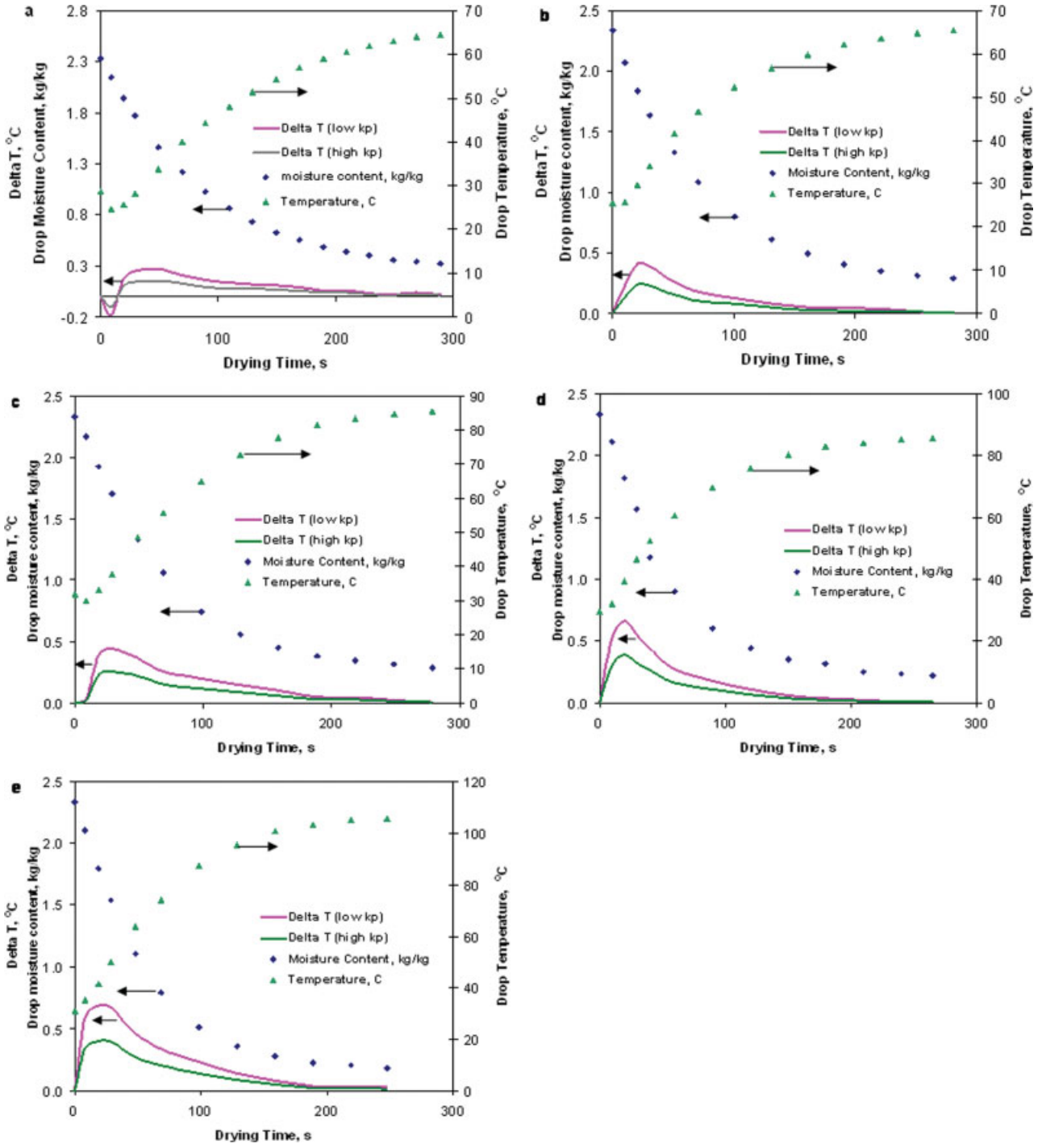

Figure 2. Predicted surface-center temperature difference profiles and measured droplet temperature and moisture content profiles of the 30 wt % skim milk droplets of 1.45 mm diameter using Case-A to Case-E drying conditions (figure a to e respectively).

[Color figure can be viewed in the online issue, which is available at www.interscience.wiley.com.]

be 0.07 W m^{-1} K^{-1}.[12] This value is close to the thermal conductivity of the bulk skim milk powder tightly packed in a container,[44] and it was far lower than the thermal conductivity of skim milk solids in the single particle. The lower thermal conductivity value would overestimate surface-centre temperature differences as well as Biot numbers.

The model presented in this study incorporated the heat flux due to surface water evaporation in the boundary condition (see Eq. 8), not in the heat conduction equation. This approach has been previously considered for the convective drying of hygroscopic food materials.[14,28,45] It is expected that this approach may provide a lower estimate of tempera-

Table 2. The Maximum Surface-Centre Temperature Difference with and without the Porosity Effect for the Case-A to Case-E Drying Conditions

Case	ΔT_{max} without Porosity (°C)	ΔT_{max} with Porosity (°C)
A	0.16	0.27
B	0.24	0.41
C	0.26	0.44
D	0.39	0.66
E	0.40	0.69

ture difference inside the droplet (ΔT). The highest estimate of ΔT should happen when the droplet surface is assumed to be fully dried, whereas the wet core is made of pure water, and the evaporation is assumed to occur from the sharp interface (at a distance somewhat away from the particle surface). The later phenomenon is unlikely to happen during the drying of hygroscopic materials such as skim milk that has little fat and is mostly made of lactose and water soluble proteins. Evaporation may start to happen within the matrix of the droplet/particle once the solids start to appear on the surface (i.e. when the porous structure is

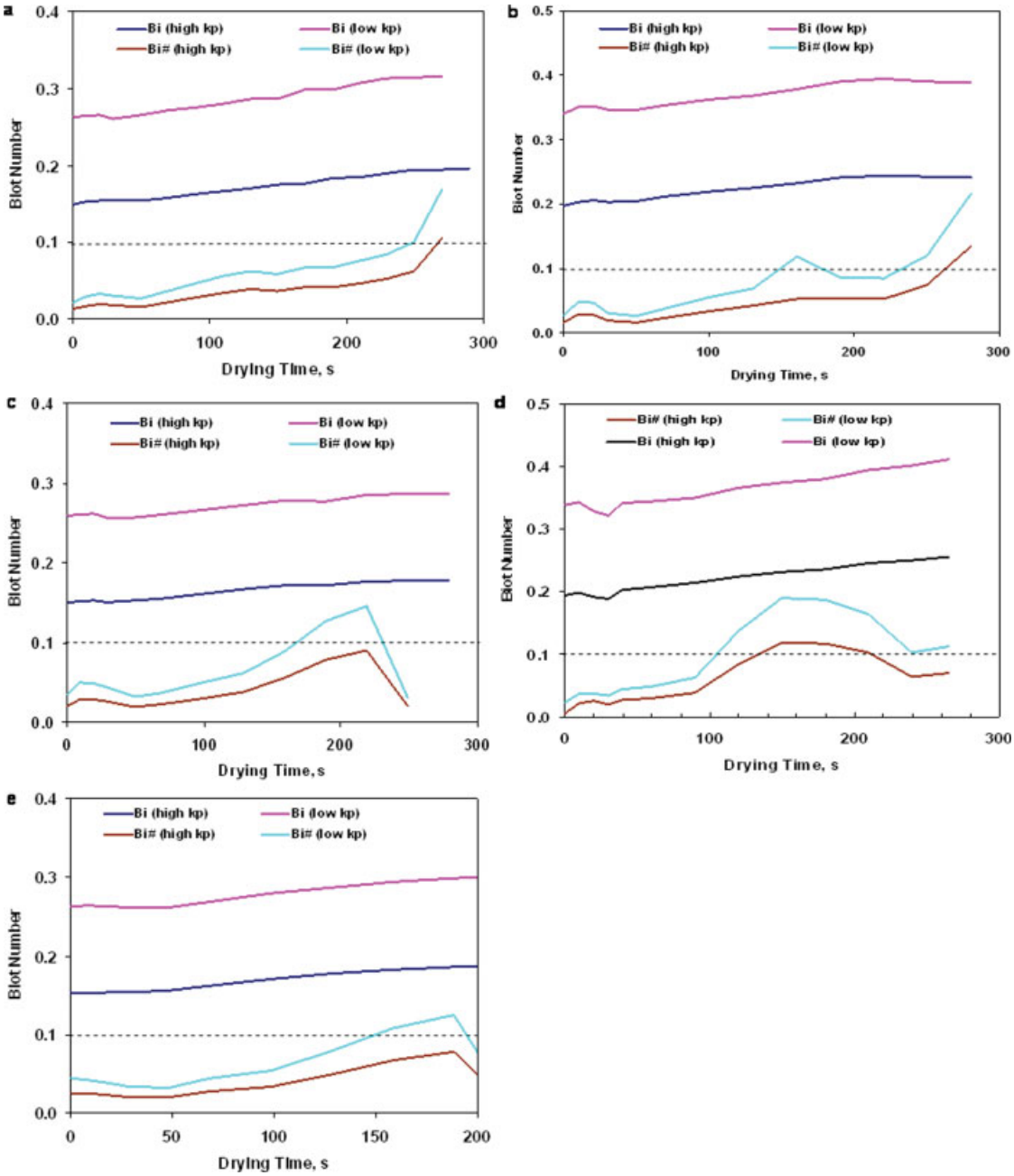

Figure 3. Drying-based and conventional Biot numbers profiles for the 30 wt % skim milk droplets of 1.45 mm initial diameter using Case-A to Case-E drying conditions (figure a to e respectively).

[Color figure can be viewed in the online issue, which is available at www.interscience.wiley.com.]

present), creating a finite surface drying region immediately next to the particle-air interface. For the 30 wt % skim milk droplet, the drying rate during the earlier drying stage or during the period of first 40% water removal was observed to be similar to that of pure water evaporation.[29] This observation is supported by the diameter profiles of pure water droplets and skim milk droplets under isothermal drying conditions, reported by Lin and Chen.[29] This indicates that a large portion of the moisture is removed from the droplet when the evaporation happened at the droplet surface or near the surface region. In other words, the drying region during the earlier drying stage is narrow.[14] Therefore, the assumption of evaporation from the droplet surface is reasonable and would not disqualify the approach. As such, the current analysis can give a realistic estimate of the temperature nonuniformity within the droplet/particle, assisting to quantitatively verify the assumption of uniform temperature during the drying of small droplets.

Predicting the biot numbers

The conventional and drying-based Biot numbers (refer to Eqs. 24 and 25, respectively) are estimated in this section to assess their differences in relation to the justification of the uniform temperature assumption. The Biot numbers were calculated for the same five drying cases (see Table 1) and using two thermal conductivity bounds, yielding two estimates of the Biot numbers. A gradual change in the Biot number during drying would occur between these lower and higher bounds. Biot number profiles following the entire drying process for Case-A to Case-E drying conditions are illustrated in Figure 3.

Results showed that the drying-based Biot numbers ($Bi^{\#}$) were smaller than the conventional Biot numbers (Bi) for all sets of drying conditions tested. Furthermore, the $Bi^{\#}$ was smaller than the critical value of 0.1 during majority of the drying period. It was observed that the $Bi^{\#}$ marginally exceeded the critical value at the end of the drying process. However, crossing the critical Biot number limit did not have a significant influence because surface-centre temperature differences were found to be negligible at the end of drying. Small drying-based Biot numbers thus favor the uniform temperature within the skim milk droplet under drying conditions used in this study. In contrast, the conventional Biot numbers were observed to be somewhat greater than the critical value of 0.1, mainly during the later drying stage.

A significant difference was observed in the conventional Bi profiles using two thermal conductivity bounds for each drying case, whereas the difference was only minor for the drying-based $Bi^{\#}$ profiles. This is because the $Bi^{\#}$ is not only affected by the droplet radius, the mean thermal conductivity and the average heat transfer coefficient, but also by the drying rate and the difference between drying gas and droplet surface temperatures. Therefore, the reduction in the droplet's thermal conductivity during drying may not necessarily lead to a drastic increment in the Biot number. The Biot number profiles also demonstrated that the drying-based $Bi^{\#}$ was not significantly increased at higher air temperature conditions unlike the conventional Bi. This is because the drying rate was greater at higher air temperature conditions, thus compensating the high temperature effect when predicting the drying-based Biot numbers. The second term on the right hand side of the Eq. 22 plays an important role to yield predictions under evaporation conditions. The drying-based Biot number seemed to capture the evaporative effect on the temperature distribution within the droplet during drying. Thus, the drying-based Biot number is more appropriate when modeling the droplet drying process.

It is clear from the predictions in this study that the Biot numbers are not very large even when the droplet's thermal conductivity is low at the end of drying. Because all parameters contributing to the Biot numbers are time-dependent during the real drying process, the net effect of these parameters to the Biot numbers is different when compared with the effect produced by the receding interface model, which appeared to "fix" the thermal conductivity, the droplet diameter, and the particle moisture content during drying. Small Biot numbers and surface-centre temperature differences predicted in this study suggest that the evaporation of moisture only from the sharp receding interface, "fixing" the droplet diameter after the constant drying-rate period and "fixing" the particle thermal conductivity in the later drying stage may not be appropriate during modeling the temperature nonuniformity within the droplet under evaporation conditions.

Table 3. Industrial Spray Drying of Skim Milk Based on 200 μm Initial Droplet Diameter

Drying Parameter/Droplet Characteristics	Inlet	Outlet
Air temperature (°C)		
20 wt % skim milk	225	73.5
30 wt % skim milk	225	83.8
50 wt % skim milk	200	82.5
Air absolute humidity (g water/kg dry air)		
20 wt % skim milk	8.0	65.4
30 wt % skim milk	8.0	60.1
50 wt % skim milk	8.0	48.8
Average drop temperature (°C)		
20 wt % skim milk	40.0	73.4
30 wt % skim milk	40.0	83.7
50 wt % skim milk	40.0	82.4
Average drop diameter (μm)		
20 wt % skim milk	200	105.5
30 wt % skim milk	200	120.7
50 wt % skim milk	200	147.4
Average drop moisture content (kg kg^{-1}, dry basis)		
20 wt % skim milk	4.00	0.063
30 wt % skim milk	2.33	0.039
50 wt % skim milk	1.00	0.035
Average drop thermal conductivity (W m^{-1} K^{-1})		
20 wt % skim milk	0.55	0.19
30 wt % skim milk	0.51	0.19
50 wt % skim milk	0.44	0.19
Average drop drying rate (kg m^{-2} s^{-1})		
20 wt % skim milk	4.72×10^{-2}	1.4×10^{-5}
30 wt % skim milk	4.74×10^{-2}	1.3×10^{-5}
50 wt % skim milk	3.59×10^{-2}	1.6×10^{-5}
Average heat-transfer coefficient (W m^{-2} K^{-1})		
20 wt % skim milk	546.2	760.9
30 wt % skim milk	546.2	710.2
50 wt % skim milk	557.1	630.8
Latent heat of vaporization (kJ kg^{-1})		
20 wt % skim milk	2117.1	2300.6
30 wt % skim milk	2117.1	2270.4
50 wt % skim milk	2158.1	2247.3

Inlet feed rate = 10,000 liter/hour, Initial feed solids content = 20 wt %, 30 wt %, and 50 wt % (dry basis), and inlet hot air rate = 150,000 kg h^{-1} (for 20 wt % and 30 wt % feed) and 145,000 kg h^{-1} (for 50 wt % feed).

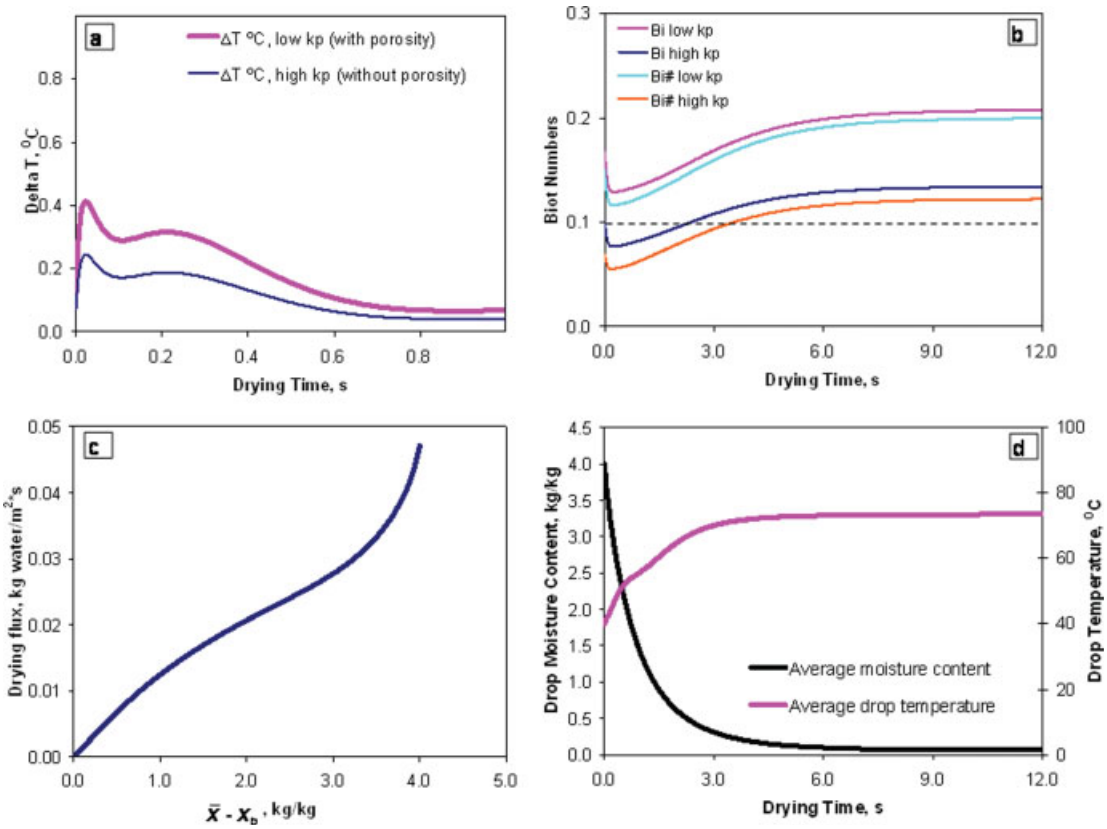

Figure 4. Droplet characteristics for industrial spray drying (see Table 3) of the 20 wt % skim milk droplets of 200 μm initial diameter: (a) surface-center temperature differences, (b) conventional and drying-based Biot numbers, (c) average drying flux, and (d) droplet moisture content and temperature.

[Color figure can be viewed in the online issue, which is available at www.interscience.wiley.com.]

Figure 3 shows that the maximum of the drying-based Biot number did not occur at the end of drying for Cases C to E, whereas for conventional Biot numbers the maximum was always noticed at the end of drying. Small peaks of the $Bi^{\#}$ profiles were due to the nature of experimental data collected from the experiment. It was observed from Figure 2 that ΔT_{max} occurred after the evaporation temperature adjustment or at the onset of the crust formation, not at the starting or end of drying. Hence, predicting Biot numbers at the beginning and end of drying may not give a true scenario about when and where the maximum temperature gradient occurs during the process. Also, the large Biot numbers at the end of drying may not necessarily indicate the high temperature gradient within the droplet/particle under drying conditions.

Calculations for the skim milk droplet of 200 μm initial diameter using industrial spray drying conditions

Experimental data considered in the above analysis used the skim milk droplets of 1.45 mm initial diameter. In industrial spray drying operations to manufacture skim milk powder, the concentrated skim milk is usually sprayed with the droplet diameter of the order of a few hundred microns. The time-dependent temperature and moisture content profiles for the drying of industrial-size droplets are not available in the literature, and are not practical to measure in the real spray dryer during manufacturing.

In this section, the Biot numbers and the surface-centre temperature difference are calculated following the single-stage drying operation. A one-dimensional dryer-wide simulation is performed here for the hot air drying of skim milk droplets of 200 μm initial diameter that is a typical droplet size in industrial-scale operations. This one-dimensional analysis would give a more realistic scenario when compared with isothermal drying of suspended droplets. The average drying rate for the skim milk droplet was estimated using the REA-based drying kinetics model briefly presented in Appendix B. During the industrial spray drying of skim milk, the concentrated feed of the 50 wt % (dry basis) initial solids content is normally used.[36] In the literature, experimental data and drying kinetics parameters (e.g. relative activation energy) were however reported for skim milk droplets of only 20 wt % and 30 wt % (dry basis) initial solids contents.[13] In this study, the relative activation energy for the skim milk droplet of the 50 wt % initial solids content is approximated using a procedure described in Appendix B.

Surface-center temperature differences and Biot numbers are calculated and compared here for the drying of skim milk droplets of 20 wt %, 30 wt % as well as 50 wt % initial solids contents. Typical hot air and skim milk characteristics during industrial operations at the inlet of the spray dryer and pre-

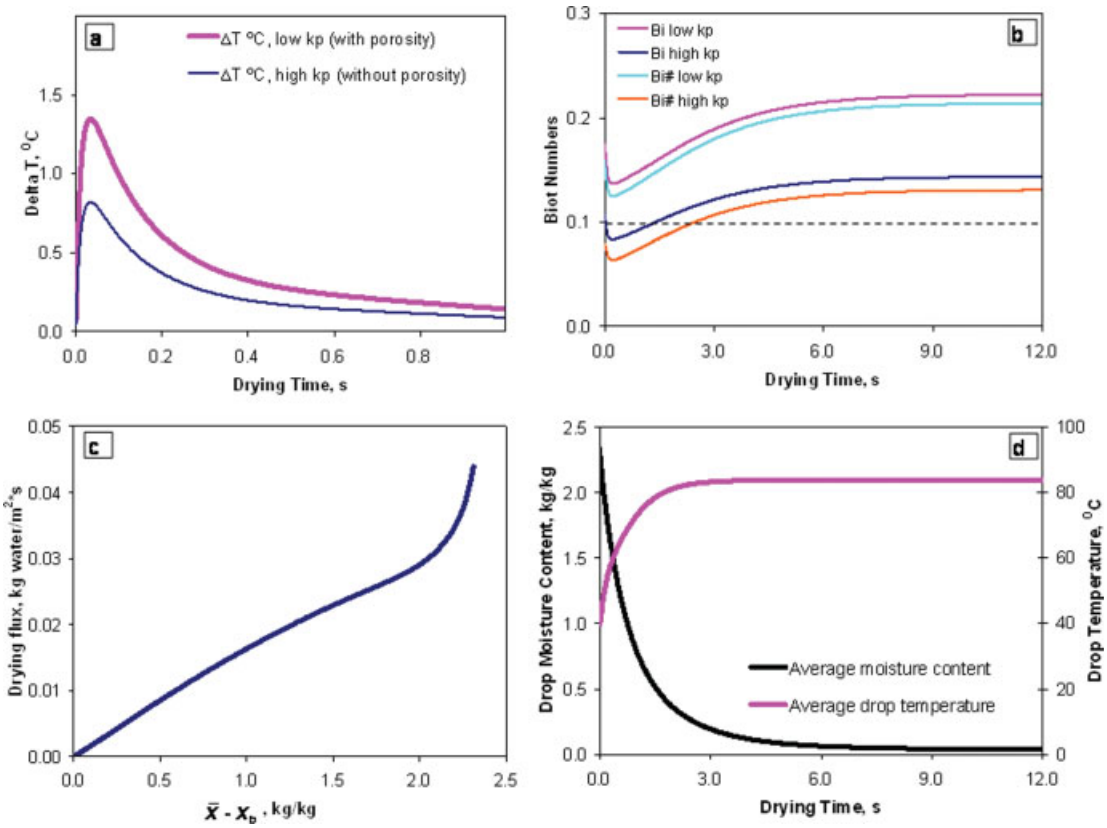

Figure 5. Droplet characteristics for industrial spray drying (see Table 3) of the 30 wt % skim milk droplets of 200 μm initial diameter: (a) surface-centre temperature differences, (b) conventional and drying-based Biot numbers, (c) average drying flux, and (d) droplet moisture content and temperature.

[Color figure can be viewed in the online issue, which is available at www.interscience.wiley.com.]

dicted gas and particle characteristics at the exit of the spray dryer are reported in Table 3. Gas properties such as temperature and humidity, and skim milk particle characteristics such as temperature, moisture content, velocity, density, and diameter were calculated over the entire drying period using heat, mass, and momentum balances illustrated in Appendix C. Changes in the droplet diameter were predicted using the perfect shrinkage model by assuming the droplet volume reduction is solely due to pure water evaporation and the droplet retains a spherical shape during the operation. Average heat-mass transfer coefficients were calculated using Ranz-Marshall correlations[46] presented in Appendix C. All other thermo-physical properties including specific heat, density, viscosity, thermal conductivity, latent heat, etc. were estimated using appropriate correlations also presented in Appendix C.

Biot numbers, surface-centre temperature differences, and other important droplet parameters such as average drying rate, moisture content, and temperature profiles are presented for the 200 μm skim milk droplet of 20 wt %, 30 wt %, and 50 wt % initial solids concentrations in Figures 4, 5, and 6, respectively. The Biot numbers and ΔT profiles were again evaluated using two thermal conductivity bounds (with and without the air-porosity effect). The average initial droplet temperature was 40°C that was smaller than the initial air wet-bulb temperature of 46.4°C. The prediction shows that ΔT at the beginning of drying was small which increased to the maximum value immediately after the wet-bulb temperature adjustment period. Because the porosity of the skim milk droplet would be negligible during the initial drying stage, predictions of ΔT with high $\overline{k}_p$ bound are likely to be more accurate. It was observed that the maximum ΔT for 20 wt % and 30 wt % skim milk droplets were 0.2°C and 0.8°C, respectively, and diminished in less than 0.6 s (see Figures 4a and 5a).

For the skim milk droplet of the 50 wt % initial solids content, the maximum ΔT was 2.3°C that rapidly reduced to less than 1°C in ~0.2 s and to less than 0.1°C in 0.5 s (see Figure 7a). ΔT for the 50 wt % droplet may appear large at the beginning of drying; however, the difference between the droplet centre and surface temperatures is only 1.44% to the difference between hot air and average droplet temperatures (200–40 = 160°C). If the initial radial velocity of the droplets for industrial operations is assumed to be 15 m/s, the temperature distribution effect within the droplet may be significant for maximum 3 m of the droplet flight. Therefore the effect of temperature nonuniformity within the droplet may not be significant for wall deposition, but may be important for agglomeration near the atomizing zone. Because the temperature distribution was only considerable for a very short drying period, it is not likely to affect the droplet's average moisture content and temperature predictions throughout the flight of droplets/particles inside the industrial spray dryer. Predictions for the 200 μm droplet also suggest that the max-

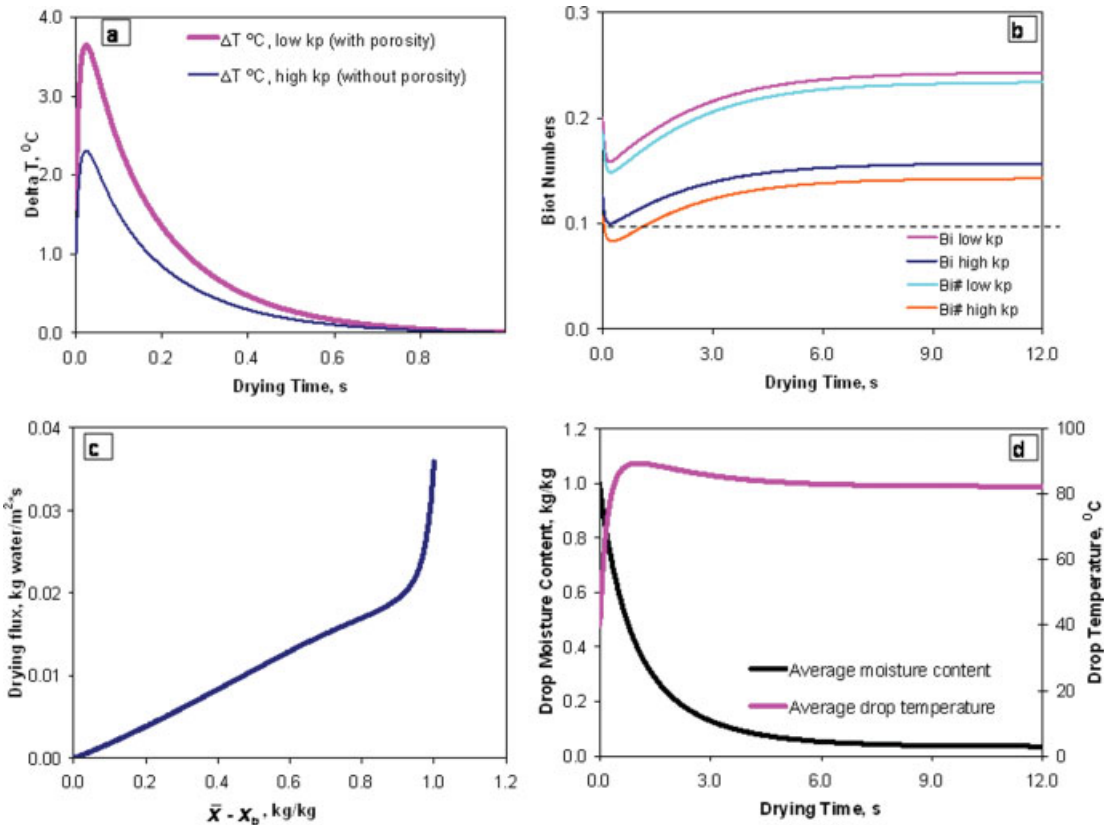

Figure 6. Droplet characteristics for industrial spray drying (see Table 3) of the 50 wt % skim milk droplets of 200 μm initial diameter: (a) surface-centre temperature differences, (b) conventional and drying-based Biot numbers, (c) average drying flux, and (d) droplet moisture content and temperature.

[Color figure can be viewed in the online issue, which is available at www.interscience.wiley.com.]

imum temperature difference occurred at the intermediate drying stage, not at the starting or end of drying.

Figures 4b, 5b, and 6b demonstrate that the drying-based $Bi^{\#}$ is around 20% smaller than the conventional Bi for skim milk droplets of 200 μm initial diameters. Both conventional and drying-based Biot numbers were less than the critical value of 0.1 at the beginning of drying for 20 wt % and 30 wt % droplets (see high $\bar{k}_p$ bounds in Figures 4b and 5b). For the 50 wt % skim milk droplet, the Biot numbers were slightly greater than the critical value (see high $\bar{k}_p$ bound in Figure 6b). Interestingly, the drying-based $Bi^{\#}$ for 50 wt% droplets was reduced to a value lower than the critical value when maximum surface-center temperature differences were observed. A sudden decline of the droplet relative velocity and hence the heat-transfer coefficient during the earlier drying stage (see Figures 4d and 5d) is responsible for the initial reduction in the drying-based $Bi^{\#}$. Prediction from this simulation illustrate that the deviation of the Biot numbers from the critical value during the later drying stage was very small even though the mean thermal conductivity of the skim milk droplet reduced from 0.44 W m^{-1} K^{-1} to 0.19 W m^{-1} K^{-1} (see average thermal conductivity values in Table 3). In essence, the small $\bar{k}_p$ at the end of drying does not guarantee the large Biot numbers or the large temperature nonuniformity within the particle.

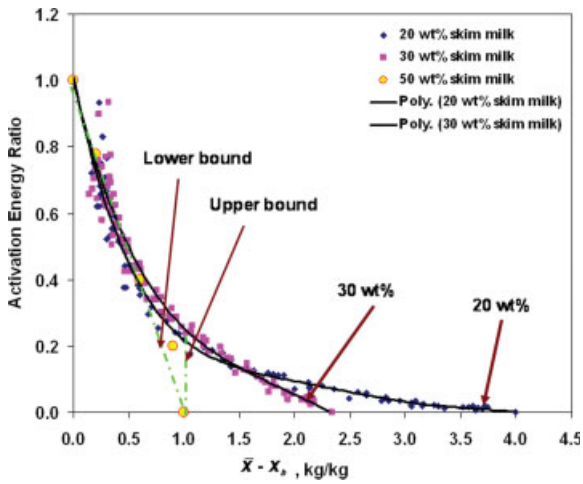

Figure 7. The relative activation energy-moisture content relationship for the 20 wt %, 30 wt %, and 50 wt % skim milk droplets using experimental data on the drying of single skim milk droplets reported by Chen and Lin.[13]

[Color figure can be viewed in the online issue, which is available at www.interscience.wiley.com.]

It is reminded that the critical value of 0.1 is used as a reference "yard-stick" which does not mean that the practical effect of small temperature distribution within the droplet/particle may be ignored in all cases. This critical value in fact depends on the maximum tolerance limit of the specific engineering scenario when accounting for the temperature effect on surface properties of some heat sensitive products. For instance, surface properties of amorphous carbohydrates (e.g. lactose) or biological solutions (e.g. liquid food with probiotics) may be significantly influenced by even small temperature differences (say 1°C). For such cases, the critical value can be made even smaller than 0.1 to be more stringent with the temperature nonuniformity within the material. Because there is no feasible experimental proof of the temperature uniformity within small droplets, it is likely that the uniform temperature assumption when $Bi^{\#} \leq 0.1$ is acceptable for heat and mass transfer calculations.

Conclusions

The receding interface model, which was widely used in the literature to estimate temperature distribution within the material, has been briefly reviewed and several limitations identified. A new approximation procedure has been described in this article to estimate the surface-centre temperature difference (ΔT) within the droplet/particle during convective drying. This approximation procedure is easy to use, requires only a few parameters for estimating surface-center temperature differences and deliver predictions over the entire drying process. The prediction in this study illustrated that the maximum temperature difference was less than 1°C for the drying of single suspended skim milk droplets under isothermal conditions (slow drying), giving the freedom of using the uniform temperature assumption in heat-mass transfer calculations. During the industrial spray drying of skim milk (fast drying), the maximum temperature difference was around 2.3°C and existed only for the short drying period. The maximum surface-centre temperature difference was observed at the onset of the crust formation on the droplet surface.

In this study, conventional and drying-based Biot numbers were estimated and compared following the complete drying process. The drying-based Biot number analysis is more appropriate when compared with the conventional Biot number analysis because the prior analysis accounts for the evaporative effect. The drying-based Biot numbers were smaller than the conventional Biot numbers under evaporation conditions. Furthermore, the drying-based Biot numbers were observed to be smaller or equal to the critical value of 0.1 for all experimental data tested, indicating the assumption of temperature uniformity within the droplet is reasonable for the practical purpose of heat-mass transfer calculations. Based on the outcomes in this work, it may be concluded that the uniform temperature assumption is reasonable for modeling the drying of small moist droplets under real spray drying conditions.

Acknowledgments

The authors gratefully acknowledge the Australian Research Council Discovery Grant (DP0773688) that has supported part of this work. The authors thank Dr. Mohit Bajaj of AMOG Consulting, Notting Hill, VIC-3168, Australia, for his help in formulating some of the initial solutions in this article.

Notation

Letters

A = surface area, m^2
B = spalding number
Bi = Biot number
$Bi^{\#}$ = drying-based Biot number
C_d = drag coefficient
C_p = specific heat, J kg^{-1} K^{-1}
d = diameter of droplet or particle, m
ΔE_v = apparent activation energy, J mol^{-1}
$\Delta E_{v,b}$ = equilibrium activation energy, J mol^{-1}
g = gravitational constant (=9.18 m s^{-2})
$\dot{G}$ = gas flow rate, kg h^{-1}
h = heat transfer coefficient, W m^{-2} K^{-1}
h_m = mass-transfer coefficient, m s^{-1}
H_b = gas enthalpy, J kg^{-1}
ΔH_L = latent heat of vaporization, J kg^{-1}
k = thermal conductivity, W m^{-1} K^{-1}
l = dryer length, m
m = mass, kg
M = molecular weight, g mol^{-1}
$\overline{N}_v$ = average drying flux, kg m^{-2} s^{-1}
Nu = Nusselt number
P = dryer pressure, kPa
Pr = Prandtl number
P_v = vapor pressure, kPa
r = radial distance in the droplet, m
R = droplet radius, m
R_g = universal gas constant (=8.314 J mol^{-1} K^{-1})
RH = relative humidity (%)
Re = Reynolds number
Sc = Schmidt number
Sh = Sherwood number
T = temperature, K
t = time, s
v = velocity, m s^{-1}
w_0 = droplet initial water mass fraction, kg kg^{-1} (wet basis)
w_b = droplet bound water mass fraction, , kg kg^{-1} (wet basis)
X = droplet moisture content, kg kg^{-1} (dry basis)
X_b = equilibrium moisture content, kg kg^{-1} (dry basis)
Y = gas absolute humidity, kg kg^{-1} (dry basis)

Greek letters

α = thermal diffusivity, m^2 s^{-1}
θ = number of droplets
μ = viscosity (Pa·s)
ε = volume fraction
ω = mass fraction
ρ = density, kg m^{-3}
ρ_v = vapor density, kg m^{-3}

Subscripts

b = bulk drying gas
da = dry air
p = particle, droplet
s = surface conditions
sat = saturated conditions
v = vapor
w = water

Literature Cited

1. Chen XD, Patel KC. Manufacturing better quality food powders from spray drying and subsequent treatments. *Drying Technol*. 2008;23:1313–1318.
2. Parti M, Palancz B. Mathematical model for spray drying. *Chem Eng Sci*. 1974;29:355–362.

3. Wijlhuizen AE, Kerkhof PJAM, Bruin S. Theoretical study of the inactivation of phosphatase during spray drying of skim milk. *Chem Eng Sci*. 1979;34:651–660.
4. Sano Y, Keey RB. The drying of a spherical particle containing colloidal material into a hollow sphere. *Chem Eng Sci*. 1982;37:881–889.
5. Cheong HW, Jeffreys GV, Mumford CJ. A receding interface model for the drying of slurry droplets. *AIChE J*. 1986;32:1334–1346.
6. Chen P, Pei DCT. A mathematical model of drying processes. *Int J Heat Mass Transfer*. 1989;32:297–310.
7. Meerdink G, van't Riet K. Prediction of product quality during spray drying. *Food Bioproducts Process*. 1995;73:165–170.
8. Zbicinski I. Development and experimental verification of momentum, heat and mass transfer model in spray drying. *Chem Eng J*. 1995;58:123–133.
9. Stevenson MJHR. *Computational modeling of drying milk droplets. Master Thesis*. The University of Auckland, New Zealand, 1999.
10. Chen XD, Pirini W, Ozilgen M. The reaction engineering approach to modeling drying of thin layer of pulped kiwifruit flesh under conditions of small Biot numbers. *Chem Eng Process*. 2001;40:311–320.
11. Langrish TAG, Kockel TK. The assessment of a characteristic drying curve for milk powder for use in computational fluid dynamics modeling. *Chem Eng J*. 2001;84:69–74.
12. Farid M. A new approach to modeling of single droplet drying. *Chem Eng Sci*. 2003;58:2985–2993.
13. Chen XD, Lin SXQ. Air drying of milk droplet under constant and time-dependent conditions. *AIChE J*. 2005;51:1790–1799.
14. Zhang J, Datta AK. Some considerations in modeling of moisture transport in heating of hygroscopic materials. *Drying Technol*. 2004;22:1983–2008.
15. Lin SXQ. *Drying of single milk droplets*. PhD Thesis. The University of Auckland, New Zealand, 2004.
16. Zbicinski I, Grabowski S, Strumillo C, Kiraly L, Krzanowski W. Mathematical modeling of spray drying. *Comput Chem Eng*. 1988;12:209–214.
17. Chen XD, Xie GZ. Fingerprints of the drying behavior of particulate or thin layer food materials established using a reaction engineering model. *Food Bioproducts Process*. 1997;75(C4):213–222.
18. van der Lijn J, Rulkens WH, Kerkhof PJAM. *Droplet heat and mass transfer under spray-drying conditions. International Symposium on Heat and Mass Transfer Problems in Engineering*. The Netherlands, 1972.
19. Adhikari B, Howes T, Bhandari BR, Troung V. Effect of addition of maltodextrin on drying kinetics and stickiness of sugar and acid-rich foods during convective drying: experiments and modeling. *J Food Eng*. 2004;62:53–68.
20. Ferrari G, Meerdink G, Walstra P. Drying kinetics of a single droplet of skim milk. *J Food Eng*. 1989;10:215–230.
21. Nešić S, Vodnik J. Kinetics of droplet evaporation. *Chem Eng Sci*. 1991;46:527–537.
22. Chou SK, Hawlader MNA, Chua KJ. Identification of the receding evaporation front in convective food drying. *Drying Technol*. 1997;15:1353–1367.
23. Silva MA. A general model for moving boundary problems—application to drying of porous media. *Drying Technol*. 2000;18:601–624.
24. Ho CK, Udell KS. Mass-transfer limited drying of porous-media containing an immobile binary-liquid mixture. *Int J Heat Mass Transfer*. 1995;38:339–350.
25. Dolinsky AA. High-temperature spray drying. *Drying Technol*. 2001;19:785–806.
26. Kuts PS, Strumillo C, Zbicinski I. Evaporation kinetics of single droplets containing dissolved biomass. *Drying Technol*. 1996;14:2041–2060.
27. Belhamri A. Characterization of the first falling rate period during drying of a porous material. *Drying Technol*. 2003;21:1235–1252.
28. Mezhericher M, Levy A, Borde I. Heat and mass transfer of a single droplet/wet particle drying. *Chem Eng Sci*. 2008;63:12–23.
29. Lin SXQ, Chen XD. Changes in milk droplet diameter during drying under constant drying conditions investigated using the glass-filament method. *Food Bioproducts Process*. 2004;82(C3):213–218.
30. Reis NC Jr, Griffiths RF, Mantle MD, Gladden LF. Investigation of the evaporation of embedded liquid droplets from porous surfaces using magnetic resonance imaging. *Int J Heat Mass Transfer*. 2003;46:1279–1292.
31. Schrader GW, Litchfield JB. Moisture profiles in a model food gel during drying: measurement using magnetic resonance imaging and evaluation of the fickian model. *Drying Technol*. 1992;10:295–332.
32. Whitaker S. Flow in porous media III: deformable media. *Transport Porous Media*. 1986;1:127–154.
33. Bramhall G. Sorption diffusion in wood. *Wood Sci*. 1979;12:3–13.
34. Patel KC, Chen XD, Kar S. The temperature uniformity during air drying of a colloidal liquid droplet. *Drying Technol*. 2005;23:2337–2367.
35. Smith JM, van Ness HC, Abbott MM. *Introduction to Chemical Engineering Thermodynamics*. New York: McGraw-Hill, 1996.
36. Písecký J. *Handbook of Milk Powder Manufacture*. Copenhagen, Denmark: Niro A/S, 1997.
37. Choi Y, Okos MR. Effects of temperature and composition on the thermal properties of foods. In: Le Maguer M, Jelen P, editors. *Food Engineering and Process Applications* (Vol.1-Transport Phenomena). New York: Elsevier, 1986:93–101.
38. Pitts DR, Sissom LE. *Schaum's Outline of Theory and Problems of Heat Transfer*. New York: McGraw-Hill, 1977.
39. Terekhov VI, Pakhomov MA, Chichindaev VV. Effect of evaporation of liquid droplets on the distribution of parameters in a two-species laminar flow. *J Appl Mech Tech Phys*. 2000;41:1020–1028.
40. Incropera FP, DeWitt DP. *Fundamentals of Heat and Mass Transfer* (5th edition). New York: Willey, 2002.
41. Chen XD, Peng X. Modified Biot number in the context of air-drying of small moist porous objects. *Drying Technol*. 2005;23:83–103.
42. Lin SXQ, Chen XD. Improving the glass filament method for accurate measurement of drying kinetics of liquid droplets. *Chem Eng Res Des*. 2002;80:401–410.
43. Bylund G. *Dairy Processing Handbook*. Lund, Sweden: Tetra Pak Processing Systems AB, 1995.
44. Al-Dabagh W. *Experimental investigation of thermal properties of particulate food materials. Master Thesis*. The University of Auckland, New Zealand, 2000.
45. Yang H, Sakai N, Watanabe M. Drying model with non-isotropic shrinkage deformation undergoing simultaneous heat and mass transfer. *Drying Technol*. 2001;19:1441–1460.
46. Chen XD. Lower bound estimates of the mass transfer coefficient from an evaporating liquid droplet—the effect of high interfacial vapor velocity. *Drying Technol*. 2005;23:59–69.
47. Chen XD. The basics of a reaction engineering approach to modelling air-drying of small droplets or thin layer materials. *Drying Technol*. 2008;26:627–639.
48. Crowe CT, Sommerfeld M, Tsuji Y. *Fundamentals of Gas-Particle and Gas-Droplet Flows*. Boca Raton, USA: CRC Press, 1998.
49. Noel DN. *Physical and Chemical Equilibrium for Chemical Engineers*. New York: Wiley, 2002.

Appendix A: Calculating the Average Thermal Conductivity of the Single Droplet/Particle

The mean thermal conductivity of single droplets at any stage of drying can be estimated using an approach considered by Choi and Okos.[37] In this approach, the droplet was assumed to be a binary system, made of solids (a mixture of various components) and water. The thermal conductivity of the liquid droplet (with no porosity) can be estimated using the thermal conductivity of solids and water:

A series model:

$$k_p = \varepsilon_{water} k_{water} + (1 - \varepsilon_{water}) k_{solids} \tag{A1}$$

A parallel model:

$$\frac{1}{k_p} + \frac{\varepsilon_{water}}{k_{water}} + \frac{1 - \varepsilon_{water}}{k_{soiids}} \tag{A2}$$

where ε is the volume fraction of individual constituents. In this study, the arithmetic average of values obtained from the series and parallel models were used as the droplet's mean thermal conductivity. The distribution factors were not incorporated because they needed to be evaluated using a regres-

sion method based on experimental measurements of thermal conductivity. The arithmetic average is considered to provide a good estimate of k_p.

Equations A1 and A2 may be used to estimate the average k_p of the "dried" particle if the porosity can be neglected in the particle matrix. When the porosity is significant in the dried particle, k_p can be estimated by incorporating the air volume fraction and the air thermal conductivity as:

A series model:

$$k_p = \varepsilon_{water} k_{water} + (1 - \varepsilon_{water} - \varepsilon_{air}) k_{solids} + K_{air} \varepsilon_{air} \quad (A3)$$

A parallel model:

$$\frac{1}{k_p} = \frac{\varepsilon_{water}}{k_{water}} + \frac{1 - \varepsilon_{water} - \varepsilon_{air}}{k_{solids}} + \frac{\varepsilon_{air}}{k_{air}} \quad (A4)$$

Again, the arithmetic average of k_p calculated by using Eqs. A3, and A4 was used as the mean thermal conductivity of the dried particle. Here, the final air porosity of the particle was taken as the volume fraction of air inside the single dried particle. The thermal conductivity of solids (k_{solids}) was calculated using the following series and parallel models[37]:

A series model:

$$k_{solids} = \varepsilon_{water} \cdot k_{water} + \varepsilon_{protein} \cdot k_{protein} + \varepsilon_{fat} \cdot k_{fat} + \varepsilon_{carbohydrate} \cdot k_{carbohydrate} + \varepsilon_{ash} \cdot k_{ash} \quad (A5)$$

A parallel model:

$$\frac{1}{k_{solids}} = \frac{\varepsilon_{water}}{k_{water}} + \frac{\varepsilon_{protein}}{k_{protein}} + \frac{\varepsilon_{fat}}{k_{fat}} + \frac{\varepsilon_{carbohydrate}}{k_{carbohydrate}} + \frac{\varepsilon_{ash}}{k_{ash}} \quad (A6)$$

The volume fraction ε_i of each constituent i can be determined using the density (ρ_i, kg m^{-3}) and the mass fraction (ω_i, wt %) of individual ingredients:

$$\varepsilon_i = \frac{\omega_i \cdot \rho}{\rho_i} \quad (A7)$$

The average particle density (kg m^{-3}) can be calculated as:

$$\rho = \frac{1}{\sum X_i / \rho_i} \quad (A8)$$

The thermal conductivity of individual ingredients was estimated using the following correlations[37]:

$$k_{water} = 0.57109 + 0.0017625 \cdot T - 6.7036 \times 10^{-6} \cdot T^2 \quad (A9)$$

$$k_{protein} = 0.17881 + 0.0011958 \cdot T - 2.7178 \times 10^{-6} \cdot T^2 \quad (A10)$$

$$k_{fat} = 0.18071 + 0.0027604 \cdot T - 1.7749 \times 10^{-7} \cdot T^2 \quad (A11)$$

$$k_{carbohydrate} = 0.20141 + 0.0013874 \cdot T - 4.3312 \times 10^{-6} \cdot T^2 \quad (A12)$$

$$k_{ash} = 0.32962 + 0.0014011 \cdot T - 2.9069 \times 10^{-6} \cdot T^2 \quad (A13)$$

Here, T (°C) is the local absolute temperature and k_i (W m^{-1} K^{-1}) is the thermal conductivity of individual constituents. The density (kg m^{-3}) of individual constituents was estimated using the following correlations[37] (T in °C):

$$\rho_{water} = 997.18 + 0.0031439 \cdot T - 0.0037574 \cdot T^2 \quad (A14)$$

$$\rho_{protein} = 1329.9 - 0.5185 \cdot T \quad (A15)$$

$$\rho_{fat} = 925.59 - 0.41757 \cdot T \quad (A16)$$

$$\rho_{carbohydrate} = 1599.1 - 0.31046 \cdot T \quad (A17)$$

$$\rho_{ash} = 2423.8 - 0.28063 \cdot T \quad (A18)$$

Appendix B: Droplet Drying Kinetics Using Reaction Engineering Approach (REA)

The droplet/particle's average drying rate and moisture content profiles were estimated using the REA-based drying kinetics model[13,15]:

$$-\frac{d\overline{X}}{dt} = \frac{h_m A_p}{m_s} \left(\rho_{v,sat} \exp\left(-\frac{\Delta E_v}{R \cdot T} \right) - \rho_{v,b} \right) \quad (B1)$$

where ΔE_v is the activation energy (J mol^{-1}). In the REA, the relationship between the relative activation energy ($\Delta E_v / \Delta E_{v,b}$) and the droplet's average moisture content ($\overline{X} - X_b$) was viewed as a characteristic property of the specific material. It is necessary to evaluate this characteristic property to calculate the drying rate. Here, $\Delta E_{v,b}$ is the equilibrium activation energy,[13] which was obtained using the gas temperature and the gas relative humidity as:

$$\Delta E_{v,b} = -R_g T_b \ln(RH_b) \quad (B2)$$

Chen and Lin[13] evaluated the relative activation energy relationship for the 20 wt % and 30 wt % skim milk droplets from the laboratory experiments on the hot air drying of single suspended skim milk droplets. Figure 7 illustrates this relationship, which was obtained from experimental data, and also the best-fit curves for the 20 wt % and 30 wt % skim milk droplets. It should be noted that the original REA model proposed by Chen and Lin[13] did not consider the influence of the droplet's initial moisture content on the relative activation energy. Recently, Chen[47] revealed that one should account for the initial moisture content effect during modeling the droplet drying process. Figure 7 has shown a variation of the relative activation energy for the skim milk droplets of 20 wt % and 30 wt % initial solids contents. The best-fit curves representing the relative activation energy-moisture content relationship for the 20 wt % and 30 wt % skim milk droplets are:

For 20 wt % skim milk droplets:

$$\frac{\Delta E_v}{\Delta E_{v,b}} = -6.47438 \times 10^{-03} (\overline{X} - X_b)^2 + 8.86858 \times 10^{-02} (\overline{X} - X_b)^4 - 0.471097 (\overline{X} - X_b)^3 + 1.22317 (\overline{X} - X_b)^2 - 1.62539 (\overline{X} - X_b) + 1.0092 \quad (B3)$$

For 30 wt % skim milk droplets:

$$\frac{\Delta E_v}{\Delta E_{v,b}} = 3.0318 \times 10^{-02} (\overline{X} - X_b)^4 - 0.26637 (\overline{X} - X_b)^3 + 0.85762 (\overline{X} - X_b)^2 - 1.3635 (\overline{X} - X_b) + 0.99609 \quad (B4)$$

Experimental data on the drying of skim milk droplets of the 50 wt % initial solids content are not available. However, it is known that the relative activation energy ($\Delta E_v/\Delta E_{v,b}$) should be zero at the starting point (at $t = 0$) due to the surface relative humidity being 100%, and 1 at the end of drying (at $\overline{X} = X_b$). Because of the nature of the curve, the relative activation energy-moisture content relationship for the 50 wt % skim milk droplet can be obtained using lower and upper bounds as shown in the Figure 7. The lower bound of $\Delta E_v/\Delta E_{v,b}$ for the 50 wt % skim milk droplet was obtained by a linear relationship between $\Delta E_v/\Delta E_{v,b}$ and $\overline{X} - X_b$ (from $\overline{X}_0 = 1.0$ kg kg^{-1} to $\overline{X} - X_b = 0$ kg kg^{-1}):

$$\left(\frac{\Delta E_v}{\Delta E_{v,b}}\right)_{lower\_bound} = 1 - \frac{\overline{X} - X_b}{\overline{X}_0 - X_b} \tag{B5}$$

The upper bound of $\Delta E_v/\Delta E_{v,b}$ for the 50 wt % skim milk droplet was chosen to follow the Eq. B4 as soon as the average moisture content ($\overline{X}$) varies from $\overline{X}_0 = 1.0$ kg kg^{-1} to $\overline{X} < \overline{X}_0$. Then the following equation can be used to estimate the relative activation energy for the 50 wt % skim milk droplet:

$$\frac{\Delta E_v}{\Delta E_{v,b}} = \frac{1}{2}\left[\left(\frac{\Delta E_v}{\Delta E_{v,b}}\right)_{lower\_bound} + \left(\frac{\Delta E_v}{\Delta E_{v,b}}\right)_{upper\_bound}\right] \tag{B6}$$

The average trend of the relative activation energy predicted by Eq. B6 is shown in Figure 7 as marked by "50 wt %."

Appendix C: Heat-Mass-Momentum Balance and Other Correlations used in Simulations

Heat balance over the drying gas

The heat balance was written considering θ number of droplets/particles, which receive the heat from surrounding hot gas and lose moisture in the form of vapor during a small time-step *dt*:

$$\dot{G}H_b - \dot{G}(H_b + dH_b) = [h(T_b - T_p) - \overline{N}_v\{\Delta H_L + C_{p,v}(T_b - T_p)\}]\theta A_p dt \tag{C1}$$

where H_b is the drying gas enthalpy that can be obtained from the following equation:

$$H_b = C_{p,b}T_b + \Delta H_L Y \tag{C2}$$

From Eqs. C1 and C2, the following heat-transfer model can be evaluated to calculate the drying gas temperature profile inside the dryer:

$$-\dot{G}C_{p,b}\frac{dT_b}{dl} = \frac{\theta A_p}{v_p}[h(T_b - T_p) - \overline{N}_v\{\Delta H_L + C_{p,v}(T_b - T_p)\}] + \dot{G}(\Delta H_L + C_{p,v}T_b)\frac{dY}{dl} \tag{C3}$$

Mass balance over the drying gas

Similarly, the mass balance can be presented for the drying gas which would provide the absolute gas humidity profile inside the dryer:

$$\frac{dY}{dl} = \frac{\theta}{v_p\dot{G}}\frac{dm_w}{dt} \tag{C4}$$

Momentum balance over the falling droplet/particle

$$\frac{dv_p}{dt} = \left[\left(\frac{\rho_p - \rho_b}{\rho_p}\right)g - \left\{\frac{0.75C_d\rho_b}{d_p\rho_p}(v_p - v_b)^2\right\}\right] \tag{C5}$$

where C_d is the drag coefficient. For $0.5 < Re < 1000$, the drag coefficient was estimated using the following correlation[48]:

$$C_d = \frac{24}{Re}(1 + 0.15Re^{0.687}) \tag{C6}$$

Other correlations

$$Nu = \frac{hd_p}{k_b} = \frac{2 + 0.6Re^{1/2}Pr^{1/3}}{1 + B^{0.7}} \tag{C7}$$

$$Sh = \frac{h_m d_p}{D_v} = 2 + 0.6Re^{1/2}Sc^{1/3} \tag{C8}$$

$$B = \frac{C_{p,v}(T_b - T_p)}{\Delta H_L} \tag{C8}$$

$$Re = \frac{d_p|v_p - v_b|\rho_b}{\mu_b} \tag{C10}$$

$$Pr = \frac{C_{p,b}\mu_b}{k_b} \tag{C11}$$

$$Sc = \frac{\mu_b}{\rho_b D_v} \tag{C12}$$

$$RH_b = \frac{\rho_{v,b}}{\rho_{v,sat}} \tag{C13}$$

$$\rho_{v,b} = \frac{P_v M_w}{R_g T_b} \tag{C14}$$

$$P_v = \frac{P \cdot Y}{Y + (M_w/M_b)} \tag{C15}$$

$$\rho_{v,sat} = \frac{P_{sat}M_w}{R_g T} \tag{C16}$$

Thermophysical properties

Vapor pressure at saturated conditions[49] (T in °C and P_{sat} in Torr)

$$\log P_{sat} = 7.94917 - \frac{1657.462}{T + 227.02} \tag{C17}$$

Specific heat of air-vapor mixture[40] (T in K and suitable for 295 K $< T <$ 800 K)

$$C_{p,b} = 1.9327\times10^{-10}T^4 - 7.9999\times10^{-7}T^3 + 1.1407\times10^{-3}T^2 - 0.4489T + 1057.3 \tag{C18}$$

Specific heat of water-vapor[37] (T in °C)

$$C_{p,v} = 0.0167T^2 - 0.0261T + 1866.4 \quad \text{(C19)}$$

Viscosity of air[40] (μ in MPa·s, T in K and suitable for 250 K $< T_b <$ 400 K)

$$\mu_b = -0.00003{T_b}^2 + 0.0687T_b + 0.885 \quad \text{(C20)}$$

Density of air-vapor mixture[36] (T_b in K)

$$\rho_b = \frac{353.12832}{T_b}\frac{1+Y}{1+1.6Y} \quad \text{(C21)}$$

Diffusivity of air-vapor mixture[40] (D_v in $m^2\ s^{-1}$, T in K and suitable for 293 K $< T <$ 373 K)

$$D_v = 1.963 \times 10^{-7}T - 3.33307 \times 10^{-5} \quad \text{(C22)}$$

Thermal conductivity of air-vapor mixture[40] (T in K)

$$k_b = 1.5207\times10^{-11}T^3 - 4.8574\times10^{-8}T^2 + 1.0184\times10^{-4}T - 0.00039333 \quad \text{(C23)}$$

Manuscript received Apr. 23, 2008, and revision received July 11, 2008.